

FINITE ELEMENT SIMULATION OF INTER-PLANT WEED CONTROL DEVICE IN PADDY FIELD

稻田株间除草部件有限元模拟

Wenting JIN^{1,2)}, Yuqi ZHUANSUN²⁾, Tengfei ZHUANG¹⁾, Qi LU¹⁾, Wenlong LI²⁾, Liuxuan MA^{*2)}

¹⁾ Chinese Academy of Agricultural Mechanization Sciences Group Co.,Ltd, Beijing 100083, China;

²⁾ College of Mechanical Engineering, Jiamusi University, Jiamus 154007, China

Tel: +86-15145498846; E-mail: 198053043@stu.jmsu.edu.cn

DOI: <https://doi.org/10.35633/inmateh-69-24>

Keywords: weeding machinery, inverted V-shaped component, finite element method, dynamic behavior

ABSTRACT

Mechanical weeding in paddy fields is a green and environmentally friendly way to control weeds, which has the advantages of reducing the amount of pesticides and improving the physical structure of the soil. This paper briefly describes the composition and relevant parameters of the mechanical weeding environment in rice fields. Using Creo 5.0, HyperMesh 2017, and LS-PrePost and LS-DYNA software to jointly simulate the interaction process between inverted V-shaped inter-plant weeding component and the soil in the paddy field, the single-point ALE multi-material unit algorithm is used to couple the soil and water with multiple substances, and realize the material movement between the soil and the water layer. Using the penalty function method, a fluid-solid coupling finite element modelled on the interaction between inter-plant weeding components and soil-water was established. The dynamic behavior of the interactions shows that the coupling stress increases and then decreases periodically, and the teeth of the spring cross the soil with a "bending moon (fish scale)" scratch, which can effectively avoid rice seedlings and reduce the injury rate.

摘要

稻田机械除草是一种绿色环保的控草方式，具有降低农药用量、改善土壤物理结构等优点。本文简要介绍了稻田机械除草环境组成及相关参数。运用 Creo 5.0、HyperMesh 2017 和 LS-PrePost 及 LS-DYNA 软件联合模拟了倒 V 型株间除草部件与水田土壤间的互作过程，其中，采用单点 ALE 多物质体单元算法，对土壤与水进行多物质耦合，实现了在株间除草部件扰动下土壤与水层间的物质运动；运用罚函数法建立了株间除草部件与土壤-水互作的流固耦合有限元模型。由互作动态行为过程可知：耦合应力呈先增后减周期性变化；弹齿划过土壤呈现“弯月（鱼鳞）”状划痕，可有效避让水稻秧苗，降低伤苗率。

INTRODUCTION

Compared with the numerical simulation method, the traditional experimental research method has a long cycle and is time-consuming and labor-intensive (Wu et al., 2019). Choosing the numerical simulation method for preliminary exploration and research and applying the research results to the test will greatly shorten the test period and reduce the research and development cost (Qi et al., 2020). At present, domestic and foreign scholars widely use virtual simulation methods for agricultural machinery-soil interaction problems. Commonly used 3D modeling software are CREO, SOLIDWORKS and UG (Abo-Elhor et al., 2004); ANSYS, ADAMS and ABAQUS are widely used for finite element analysis (Shinde et al., 2011). Bentaher et al. used 3D reconstruction combined with the finite element method to simulate the process of ploughing body cutting soil. The simulation results show that the best working angle of the plough body is 22° (Bentaher et al., 2013). Qi Long et al. used ANSYS software to simulate the interaction process between the paddy field raking-pressed inter-row weeding wheel and soil, and explored the effects of soil type, water depth and weeding wheel speed on the coupling stress and soil disturbance rate (Qi et al., 2015). Tian Liang et al. used the discrete element method to simulate and analyze the interaction process between the weeding wheel and the soil in paddy fields, and obtained the influence of the depth of the weeding wheel, the speed of the weeding wheel and the forward speed of the machine on the torque and soil disturbance rate, and verified through soil trough and field experiments (Tian et al., 2021).

¹ Wenting JIN, Ph.D.Stud; Tengfei ZHUANG, Engineer; Qi LU, Ph.D.Stud;

² Liuxuan MA*, Professor (Corresponding author); Yuqi ZHUANSUN, Undergraduate; Wenlong LI, Master Degree

To sum up, it is feasible to use virtual simulation method to study the interaction between agricultural machinery and soil. In this paper, the joint modeling finite element virtual simulation is used for the inverted V-shaped inter-plant weeding component, and the interaction process between the weeding component and the paddy soil coupling model is simulated, in order to improve the effect of mechanical weeding between rice fields and accelerate the process of weeding mechanization in paddy fields.

MATERIALS AND METHODS

WEEDING ENVIRONMENT AND WORKING PRINCIPLE

The inter-plant mechanical weeding environment in a rice field includes inter-plant weeding machinery, rice seedlings, weeds, soil and water, as shown in Fig 1. The row spacing is 0.2 ~ 0.3 m; the plant spacing is 0.1 ~ 0.12 m. Various weeds are randomly distributed throughout the paddy field (Jin et al., 2021). When the rice had been transplanted for about 20 days, the root depths of rice and weed were 0.08 ~ 0.1 m and 0.03 ~ 0.07 m, respectively. Paddy soil can be divided into soil layer and mud layer after soaking and beating, and the depths are 0.16 ~ 0.18 m and 0.03 ~ 0.05 m respectively (Tao et al., 2015). Different growth stages of rice seedlings have different water requirements, and the water layer is generally not more than the leaf core.

The inverted V-shaped between plant weeding device consists of a weeding claw, an inverted V mechanism and a transmission mechanism. The transmission mechanism mainly includes an inverted V-shaped transmission shaft, a transverse transmission shaft and a gear composed of a large bevel gear and two small bevel gears group. The weeding claw is the part of the device that directly contacts the soil and plants in the paddy field, and is welded by spring teeth and a claw plate. Two weeding claws are symmetrical and have a phase angle of 36° between the spring teeth of the same No.. The distance between the center of the claw plate is L, the rotation center line extends and the intersection angle α is 50°, and the shape is like an inverted V, so it is called "inverted V mechanism".

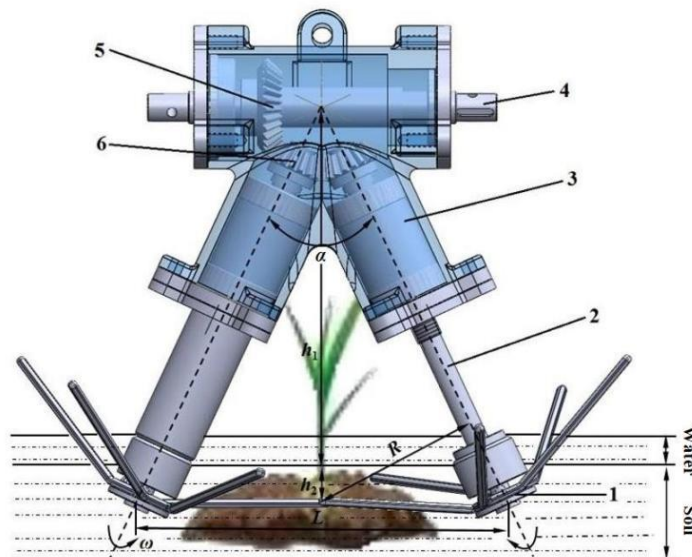


Fig. 1 - Schematic diagram of the environmental structure of mechanical weeding among rice fields

- 1. Weeding claw; 2. Inverted V-shaped drive shaft; 3. Inverted V-shaped cover;
- 4. Lateral drive shaft; 5. Large bevel gear; 6. Small bevel gear

For each row of between plant weeding operations, the weeding claws are powered by a diesel engine through a gearbox through a series of transmissions (chain transmission, gear transmission), and move in a counter-rotating trochoidal motion in the direction opposite to the machine operation. The depth of the spring teeth into the soil is h_2 . The soil is cut in sequence to muddy the water. When the spring teeth touch the main root of the rice seedling without touching the secondary root, the secondary root produces a certain pulling force on the main root and resists the partial thrust of the spring teeth, so that the growth posture of the seedling is less affected; But when the spring teeth come into contact with the secondary roots of the rice seedling, the rice seedlings move away from the soil with the spring teeth, causing damage to the seedling. Since weed has only main roots, they can easily be separated from the original floating water surface or buried in the soil, inhibiting their growth.

FINITE ELEMENT SIMULATION

The "joint modeling" is used to carry out finite element simulation analysis on the interactive relationship between paddy field weeding components and soil. The simulation process flow chart is shown in Fig. 2.

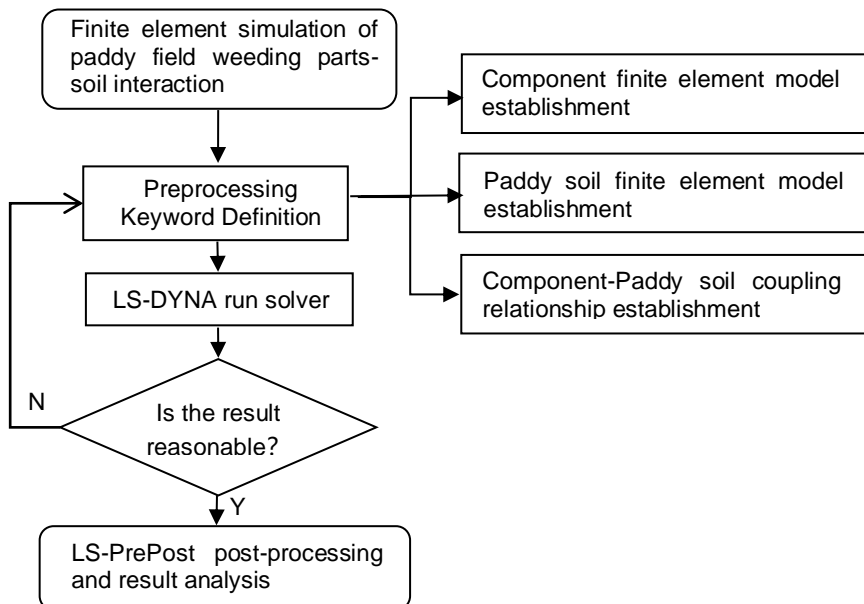


Fig. 2 - Simulation process flow chart

Establishing a finite element model of the component

Import the inter-plant weeding component model into HyperMesh software and find that the boss information of the cutter plate is missing. Select "Geom" in the page menu bar to modify and operate the inter-plant weeding component model. Click "surfaces", select the stretching command, click the missing surface (Zhou et al., 2015), select the positive direction of the Y-axis of the coordinate system as the stretching direction, set the stretching length to 4, and complete the repair of the model, as shown in Fig 3.

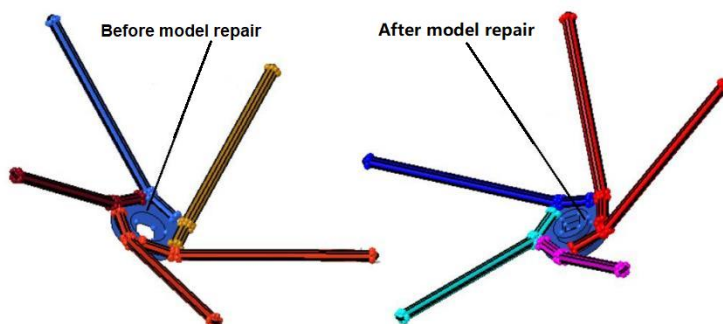


Fig. 3 - Comparison before and after model repair

Due to the different contact between the cutter plate and the spring teeth, the meshes of it are different. The cutter plate is divided into Solid meshes, and the spring teeth are divided into Shell meshes. The mesh size of the cutter plate and spring teeth is both set to 0.001 m, with a total of 31795 nodes and 31892 elements.

The inter-plant weeding component work in a high-moisture soil environment, and have strong impact under high-speed rotation and forward speed. Therefore, 65Mn spring steel with strong oxidation resistance, corrosion resistance and wear resistance is selected, and rigid material (*MAT_RAGID) is selected as the simulation material, and the parameters are set as: density 7.85×10^3 kg/m³, Young's modulus 2.1×10^3 MPa, Poisson's ratio 0.3. In addition, the degrees of freedom in the X and Z axes of the movement direction and the Y axes degrees of freedom of rotation direction are constrained, and other parameters are selected by default.

Establishing a finite element model of paddy soil

In order to ensure that the water layer and the soil share the grids and nodes on the cutting plane, and the watershed boundary is not distorted during the process of cutting the paddy field soil by the inter-plant

weeding component (*Liu*, 2020). Creo 5.0 software is used to establish a solid with length \times width \times height [soil height + water layer height (W_h : W_{h1} - W_{h2} - W_{h3})] with a size of $0.5m \times 0.6m \times [0.1+(0.01-0.04-0.07)] m$ to represent a rectangular. Then use the segmentation function to divide the model into two layers, the upper layer represents water, and the lower layer represents soil, as showed in Fig 4.

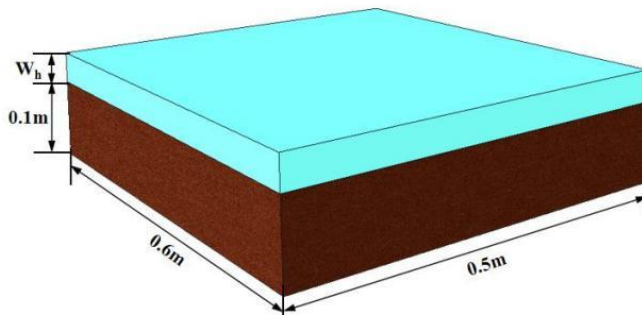


Fig. 4 - 3D model of water-soil

The soil layer material is selected from No. 147 material (*MAT_FHWA_SOIL) in the material library. The main parameters are set according to the paddy soil parameters in Table 1, and the default values are selected for other parameters. The soil failure criterion of paddy field generally adopts the Mohr-Coulomb yield criterion (M-C criterion) (*Yang.*, 2014) with the addition of the similar factor modified Drucker-Prager criterion (D-P criterion), as showed in formula (1):

Table 1

Soil parameters of sampling paddy field

Soil density [g/cm ³]	Moisture content [%]	Cohesive strength [MPa]	Friction angle [°]	Bulk modulus [MPa]	Poisson's ratio	Shear modulus [MPa]
1.681	68.3	0.0037	19.022	21.8	0.51	7.22

$$F = -p \sin \phi + \sqrt{J_2 K(\theta)^2 + \alpha^2 \sin^2 \phi} - c \cos \phi = 0 \quad (1)$$

$$K(\theta) = \cos \theta + \frac{1}{\sqrt{3}} \sin \theta \cos \phi \quad (2)$$

where:

F is the model surface yield force, N; P is the pressure, MPa; ϕ is the Friction angle, °; J_2 is the second invariant of deviatoric stress; α is the similarity factor between the corrected yield surface and the standard M-C yield surface; c is the cohesive strength, MPa.

The upper layer of the model is actually a mixture of water and various substances. In order to facilitate the definition of simulation parameters, the upper layer is water by default. No. 9 material (*MAT_NULL) in the material library is selected for the water layer. This material is an empty material model, which can provide movement space for the soil, which is suitable for the large deformation problem of cutting soil by weeding parts between plants (*Zhao.*, 2017). The pressure-volume relationship of the water layer adopts the Grüneisen equation of state, as shown in formula (3):

$$P = \frac{\rho C^2 \mu \left[1 + \left(1 - \frac{\gamma_0}{2} \right) \mu - \frac{\alpha_2 \mu^2}{2} \right]}{\left[1 - (S_1 - 1)\mu - \frac{S_2 \mu^2}{\mu + 1} - \frac{S_3 \mu^3}{(\mu + 1)^2} \right]} + (\gamma_0 + \alpha_2 \mu) E \quad (3)$$

$$\mu = \frac{\rho}{\rho_0} - 1 \quad (4)$$

where:

ρ is the density of water, g/cm³; C is the impact velocity-particle velocity curve intercept; S_1 , S_2 and S_3 are the impact velocity-particle velocity curve coefficients; μ is volume strain; E is the initial energy, J/Kg; γ_0 is the Grüneisen constant; α_2 is the order volume correction factor.

Using the single-point ALE multi-material unit body algorithm in the ALE method, and using the keyword *ALE_MULTI_MATERIAL_GROUP to perform multi-material fluid-structure coupling on the soil layer and the water layer. The two are bound in a unit algorithm to realize the material exchange and transportation between water and soil (Wang et al., 2021).

Establishment of fluid-solid coupling relationship between components and paddy soil

After completing the finite element model of the inter-plant weeding component and the paddy soil, it is necessary to establish the fluid-solid coupling relationship between the two to solve. Use the keyword *CONSTRAINED_LAGRANGE_IN_SOLID to define the contact form between the inter-plant weeding components and the paddy field-soil, set the Lagrange unit (a pair of inter-plant weeding components) as SLAVE, the ALE multi-substance unit (soil-water) as MASTER, and set the kinetic friction coefficient as 0.1, the static friction coefficient as 0.5, and other parameters are selected as default.

The penalty function method is used to perform fluid-solid coupling between the inter-plant weeding component and the paddy field soil. This method can track the relative displacement between the inter-plant weeding component and the paddy field soil, and detect whether penetration occurs on the paddy field soil surface, so that the system maintains kinetic energy conservation (Wang et al., 2021).

In the fluid-structure interaction, the Lagrange dynamic equation is adopted, such as formula (5):

$$M\ddot{U} + D\ddot{U} + KU = F^S + F^{FSI} \quad (5)$$

where:

M is the mass matrix of the Lagrange unit cell, kg;

D is the damping matrix of the Lagrange unit cell, N/(m/s);

\ddot{U} is the acceleration of the Lagrange unit cell, m/s²;

K is the stiffness matrix of Lagrange unit cell, N/m;

U is the displacement of the Lagrange unit cell, m;

F^S is the external load vector without fluid force;

F^{FSI} is the coupled stress of the fluid acting on the Lagrange unit cell, which can be expressed by formula (6).

$$F^{FSI} = - \int_{\Gamma_{FSI}} N^T n_f \sigma_f d\Gamma \quad (6)$$

where:

Γ_{FSI} is the fluid-solid coupling contact surface, which can be deformed; N^T is the velocity interpolation matrix after transposition; n_f is the outer normal vector of the fluid domain Neumann boundary unit; σ_f is the Cauchy stress tensor within the fluid.

In order to simulate the infinite space of real paddy soil, all the degrees of freedom at the bottom of the paddy soil model are constrained, and non-reflection boundary conditions are added to the other five surfaces. In addition, to achieve the purpose of mutual transport between soil and water, the keyword *CONTROL_ALE is defined, as showed in Fig 5.

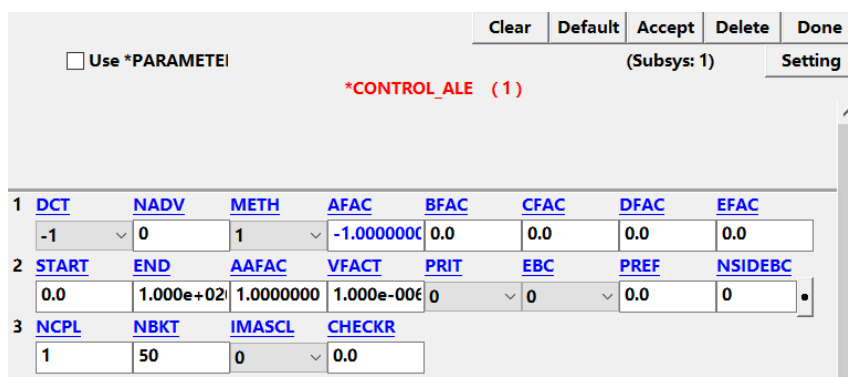


Fig. 5 - ALE control algorithm parameters

Combined with the coupled stress-time curve diagram (as shown in Fig 6) and the coupled stress nephogram (as shown in Fig 7), the stress field of the finite element simulation model of the interaction between the inter-plant weeding component in the paddy field and the soil is analyzed, and it is known that: The inter-

plant weeding component in the paddy field cuts the paddy field soil inward. Under the cutting disturbance of the inter-plant weeding component, the water-soil coupling interface is destroyed, resulting in coupling stress.

When $t_1=0.028$ s, the No. 0 spring tooth of the right inter-plant weeding component cuts the coupling interface, and the tooth tip completely enters the soil, and the coupling stress reaches the first peak point of 0.5134 MPa, as shown in Fig 7 - a); When $t_2=0.073$ s, the No. 0 spring tooth of the left inter-plant weeding component cuts the coupling interface, and the tooth tip completely enters the soil, and the coupling stress reaches the second peak point of 0.5555 MPa, as shown in Fig 7 - b); When $t_3=0.110$ s, the No. 1 spring tooth of the right inter-plant weeding component cuts the coupling interface, and the tooth tip completely enters the soil, and the coupling stress reaches the third peak point of 0.5490 MPa, as shown in Fig 7 - c); When $t_4 = 0.142$ s, the No. 1 spring tooth of the left inter-plant weeding component cuts the coupling interface, and the tooth tip completely enters the soil, and the coupling stress reaches the fourth peak point of 0.5543 MPa, as shown in Fig 7 - d).

RESULTS

The results after the operation was solved, were imported into LS-PrePost 4.3 for dynamic behavior analysis. In order to facilitate the observation of the dynamic behavior of the inter-plant weeding components in the soil, the water layer was hidden, and the stress and density of the water layer-soil coupling interface were selected to analyze the stress field and flow field of the interaction process of the inter-plant weeding component in the paddy field soil.

Stress Field Analysis

Combined with the coupled stress-time curve diagram (as shown in Fig. 6) and the coupled stress nephogram (as shown in Fig.7), the stress field of the finite element simulation model of the interaction between the inter-plant weeding component in the paddy field and the soil is analyzed, and it is known that: the inter-plant weeding component in the paddy field cuts the paddy field-soil inward. Under the cutting disturbance of the inter-plant weeding component, the water-soil coupling interface is destroyed, resulting in coupling stress.

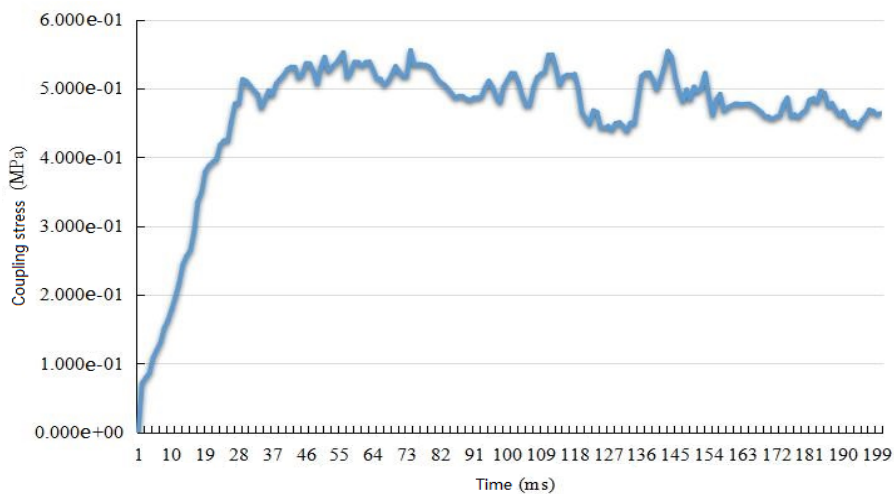


Fig. 6 - Coupling stress-time graph

When $t_1=0.028$ s, the No. 0 spring tooth of the right inter-plant weeding component cuts the coupling interface, and the tooth tip completely enters the soil, and the coupling stress reaches the first peak point of 0.5134 MPa, as shown in Fig 7 - a); When $t_2=0.073$ s, the No. 0 spring tooth of the left inter-plant weeding component cuts the coupling interface, and the tooth tip completely enters the soil, and the coupling stress reaches the second peak point of 0.5555 MPa, as shown in Fig 7 - b); When $t_3=0.110$ s, the No. 1 spring tooth of the right inter-plant weeding component cuts the coupling interface, and the tooth tip completely enters the soil, and the coupling stress reaches the third peak point of 0.5490 MPa, as shown in Fig 7 - c); When $t_4 = 0.142$ s, the No. 1 spring tooth of the left inter-plant weeding component cuts the coupling interface, and the tooth tip completely enters the soil, and the coupling stress reaches the fourth peak point of 0.5543 MPa, as shown in Fig 7 - d).

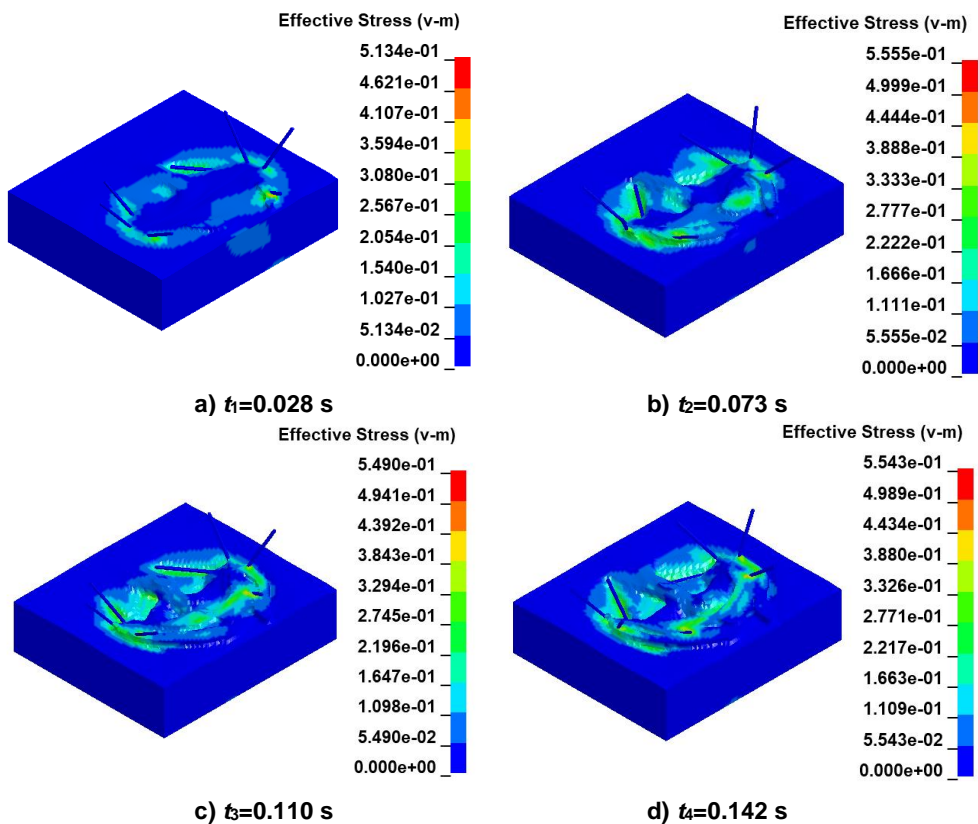


Fig. 7 - Coupling stress cloud diagram

Flow field analysis

The water-soil model adopts the single-point ALE multi-substance unit algorithm, and the simulation model is a fluid state. By observing the water-soil fluid flow change diagram (as shown in Fig 8) and the soil density-time curve (as shown in Fig 9), the flow field of the finite element simulation model of paddy field weeding component-soil interaction is analyzed, and it is known that: since the fluid-structure coupling keyword is defined between the water layer and the soil, the water and soil can flow freely and exchange substances. Therefore, under the disturbance of the rotating spring teeth of the inter-plant weeding component, the soil grid contacted by the spring teeth is destroyed, the soil is forced to flow backward and upward, and the water flows downward to the space where the soil is destroyed. Each spring tooth scratches the soil to present a "meniscus (fish scale)" -like scratch, and the water molecules and soil particles are mixed and stirred to make the water layer turbid.

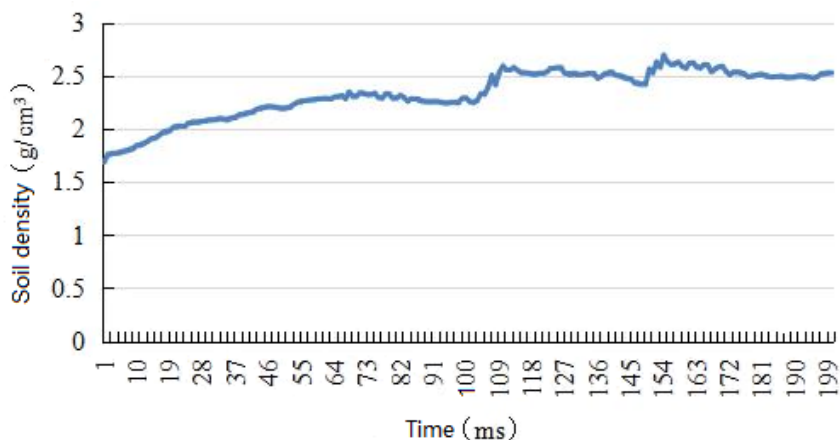
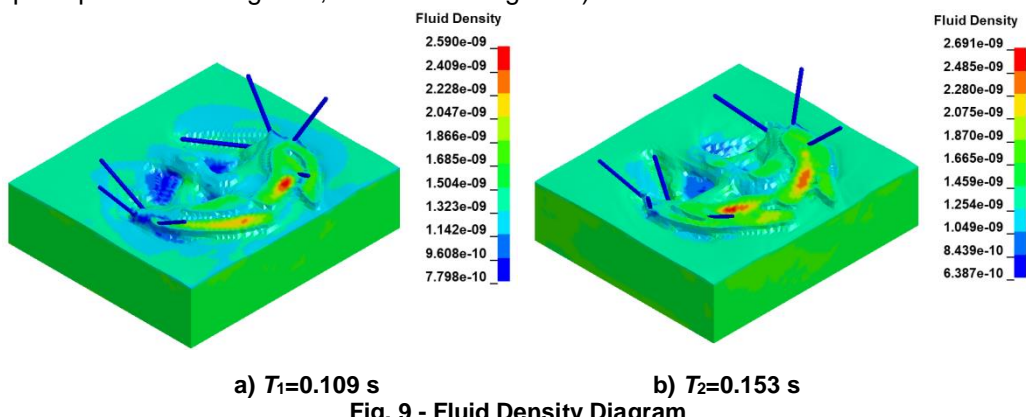


Fig. 8 - Soil density-time curve diagram

When $T_1=0.109\text{ s}$, the No. 0 spring tooth of the right inter-plant weeding component has just crossed the lowest point of rotation, and the No. 0 spring tooth of the left inter-plant weeding component is about to reach the lowest point of rotation.

The soil is flowing backwards and upwards accumulated in the water layer to form the first "meniscus (fish scale)"-shaped bulge. At this time, the No. 4 spring tooth of the right inter-plant weeding component just rotated and impacted this watershed. Make the density of fluid (soil) reach the first peak point of 2.590 g/cm^3 , as shown in Fig 9 - a); When $T_2=0.153 \text{ s}$, the No. 1 spring tooth of the right inter-plant weeding component is about to reach the lowest point of rotation, and the soil is transported backward and upward to accumulate in the water layer to form a second "meniscus (fish scale)"-shaped bulge. At this time, the No. 4 spring tooth of the left inter-plant weeding component just rotated and impacted the watershed, and fluid (soil) density reached the second peak point of 2.691 g/cm^3 , as shown in Fig 9 - b).



CONCLUSIONS

(1) Using the idea of "joint modeling", the material exchange between the soil and the water layer was realized under the disturbance of the inter-plant weeding component; the dynamic behavior process of the inter-plant weeding component and the soil was established and analyzed.

(2) Through the analysis of the stress field, it can be concluded that when the spring tooth cuts the coupling interface and the tooth tip completely enters the soil, the interface coupling stress is the largest. Because the paddy soil has a certain fluidity, compactness around the soil decreases under the disturbance of the previous spring teeth, and the coupled stress first increases and then decreases cyclically during the forward movement of the inter-plant weeding components. The lower the coupling stress, the lower the resistance of the inter-plant weeding components during weeding operation and the lower the power consumption of the machine.

(3) Through the analysis of the convective flow field, it can be concluded that during the rotation of the inter-plant weeding components, the lower end of the soil grid is not damaged because it is not in direct contact with the spring teeth, but is compressed by downward pressure. In addition, the soil is forced to flow backwards and upwards, and accumulates and squeezes in a certain watershed of the water layer, which makes the fluid density increase. The greater the variation in fluid density, the greater the rate of soil disturbance and the greater the rate of weed control during inter-plant weeding component operation.

ACKNOWLEDGEMENT

This work was supported by the Natural Science Foundation of Heilongjiang Provincial (No. LH2020E026), National Modern Agricultural Industrial Technology System Construction Special Fund (No. CARS-01) and the Basic Scientific Research Business Expenses of the Department of Education of Heilongjiang Province (No. 2019-KYYWF-1378).

REFERENCES

- [1] Abo-Elnor M., Hamilton R., Boyle J.T. (2004) Simulation of soil-blade interaction for sandy soil using advanced 3D finite element analysis[J]. *Soil and Tillage Research*, 75(1): 61-73.
- [2] Bentaher H., (2013). Finite element simulation of moldboard-soil interaction. *Soil & Tillage Research*, Vol. 134, pp. 11-16.
- [3] Jin W.T., Ge Y.Y., Fan W.W. et al., (2022). Virtual simulation and verification of inverted V-shaped inter-plant weeding device for paddy field (倒 V 型稻田株间除草装置虚拟仿真及验证). *Journal of Chinese Agricultural Mechanization*, Vol. 43, Issue 10, pp. 72-77.
- [4] Liu X.D., (2020). *Development and experiment of combined operation machine for split deep rotary tillage and soil disinfection* (分体式深旋耕土壤消毒联合作业机研制与试验). [D], Jiangsu University.

- [5] Qi L, Liang Z W, Ma X., (2015). Validation and analysis of fluid-structure interaction between rotary harrow weeding roll and paddy soil (耙压式除草轮与水田土壤作用的流固耦合仿真分析及验证). *Transactions of the Chinese Society of Agricultural Engineering*, Vol. 31, Issue 05, pp. 29-35+37+36.
- [6] Qi L., Liu C., Jiang Y. et al., (2020). Present status and intelligent development prospects of mechanical weeding technology and equipment for rice (水稻机械除草技术装备研究现状及智能化发展趋势). *Journal of South China Agricultural University*, Vol.41, Issue 06, pp. 29-36.
- [7] Shinde G.U., Kajale S.R. (2011) Computer aided engineering analysis and design optimization of rotary tillage tool components [J]. *International Journal of Agricultural and Biological Engineering*, 4(3): 1-6.
- [8] Tian L., (2021). Design and test of post-seat weeding machine for paddy. *Int. J. Agric & Biol Eng*, Vol.14, Issue 03, pp. 112–122.
- [9] Tao G.X., Wang J.W., Zhou W.Q. et al., (2015). Herbicidal mechanism and key components design for paddy weeding device (水田株间除草机械除草机理研究与关键部件设计). *Transactions of the Chinese Society for Agricultural Machinery*, Vol.46, Issue 11, pp. 57-613.
- [10] Wang Q., Zhou W.Q., Tang H. et al., (2021). Design and Experiment of Arc-tooth Reciprocating Motion Type Seedling Avoided Weeding Control Device for Intertillage Paddy (弧齿往复式稻田株间自动避苗除草装置设计与试验). *Transactions of the Chinese Society for Agricultural Machinery*, Vol.52, Issue 06, pp. 53-61+72.
- [11] Wang J.W., Ma X..C, Tang H. et al., (2021). Design and Experiment of Curved-tooth Oblique Type Inter-row Weeding Device for Paddy Field (曲面轮齿斜置式稻田行间除草装置设计与试验). *Transactions of the Chinese Society for Agricultural Machinery*, Vol.52, Issue 04, pp. 91-100.
- [12] Wu T., Zeng S., Zhao R.M. et al., (2019). Analysis and study on intelligentized technologies of intra-row weeding mechanical control (智能化作物株间机械除草技术分析与研究). *Journal of Agricultural Mechanization Research*, Vol.41, Issue 06, pp. 1-6+12.
- [13] Yang J., (2014). *Validation and analysis of fluid-structure interaction between rotary harrow weeding roll and paddy soil* (基于扩展有限元法和离散元法的土壤-耕具接触研究). Master dissertation, Kunming University of Science and Technology.
- [14] Zhou X.Q., Zhang J., Xiao J. et al., (2015). Simulation of cutting process with double disc colter based on LS-dyna (基于LS—dyna的双圆盘开沟器切削过程的仿真). *Journal of Chinese Agricultural Mechanization*, Vol.36, Issue 05, pp. 288-291+307.
- [15] Zhao L.L., (2017). *Study on the key technology of riding paddy field cultivator* (乘坐式水田中耕除草关键技术研究). Master dissertation, South China Agricultural University.